Fuel 303 (2021) 121278

Contents lists available at ScienceDirect

Fuel

journal homepage: www.elsevier.com/locate/fuel

Full Length Article

Fickian diffusion in CO_2 injection: A two-phase compositional flow model with fully 3D unstructured gridding

Ali Zidane [a], Abbas Firoozabadi [a,b,*]

[a] Reservoir Engineering Research Institute (RERI), Palo Alto, CA, USA
[b] Chemical and Biomolecular Engineering Department, Rice University, Houston, TX, USA

ARTICLE INFO

Keywords:
CO_2 injection
Fickain diffusion
Unstructured gridding
Implicit scheme
Two-phase
Compositional
Peng-Robinson EOS
Newton-Raphson
3D simulation

ABSTRACT

We present numerical modeling of CO_2 injection in lab and field scales using fully unstructured grids with Fickian diffusion. The focus is on CO_2 injection because of its wide range of applications and environmental and economic benefits. We demonstrate predictions of experimental measurement results without tuning and/or adjustment of Fickian diffusion coefficients and flow parameters. The spatial and temporal discretization in the algorithm allows for accurate description of the physics of the flow. Unstructured gridding at the lab scale simulation increases accuracy of Fickian diffusion flux computations. In this work we also compare the efficiency and accuracy of our algorithm to two-point and multi-point flux approximations. A grid sensitivity analysis demonstrates low mesh dependency of the model.

1. Introduction

Reservoir simulation of flow processes in complex reservoirs is an important tool in the investigation of various fluid injection schemes. Examples of applications include gas injection in oil reservoirs and recycling in rich gas condensate reservoirs where the subsurface may be heterogeneous. Specific examples are CO_2 injection, potentials from enhanced oil recovery, and sequestration with its accompanying climate benefits. Simulation of CO_2 injection in the subsurface has much more complexities than hydrocarbon gas injection due to various density effects as will be demonstrated in this paper.

Reservoir simulation is based on division of a physical domain into grid-blocks. Current gridding approaches are generally Cartesian, approximately Cartesian, and Voronoi/perpendicular bisector (PEBI) grids [1–3]. In this work the terms “mesh” and “grids” are used interchangeably. The Cartesian gridding [4,5] and in general gridding that includes pillars or vertical structure may not allow the capture of geologic details [1]. Unstructured gridding allows to include the architecture of the formation to be included and allows realistic description of the physical domain [6–9]. There is a limited literature on unstructured gridding in compositional multiphase flow compared to a vast literature on structured gridding [10]. In [11] the authors present a model for compositional simulation on unstructured gridding with an explicit time discretization scheme. In [10] the authors propose an equation of state-based implicit simulator applied in Voronoi type unstructured gridding. The Voronoi grids are superior to structured grids; however, their application is limited to 2.5 D. The use of Cartesian gridding in complex formations may be inefficient. In [12] it is concluded that the techniques associated with Cartesian grids (such as local grid refinements (LGR)) in complex reservoirs make the simulation impractical. LGR in areas of interest may require significantly finer gridding and consequently higher CPU time and memory. In addition, Cartesian LGR [13] and hybrid LGR do not align with the grid lines in complex formations [14]. In an alternative approach, the hybrid grid generation is presented in [15] where the finite difference (FD) grids around the faults are replaced with tetrahedra. This technique is known as the locally unstructured gridding [15–18]. It overcomes the limitations of traditional full FD gridding, but it retains the FD character of the simulation. In this work we demonstrate that efficiency and accuracy can be achieved in complex domains discretized by fully unstructured gridding [39].

The two-point flux approximation (TPFA) does not converge to the correct solution on non *K*-orthogonal meshes [19]. When coupled with the finite difference (FD) and finite volume (FV) approaches, excessive numerical dispersion and grid sensitivity is observed caused by the single up-winding scheme [20]. Those issues become critically important in compositional flow where phase behavior depends on the

* Corresponding author.
E-mail address: af@rerinst.org (A. Firoozabadi).

https://doi.org/10.1016/j.fuel.2021.121278
Received 29 April 2021; Received in revised form 13 June 2021; Accepted 14 June 2021

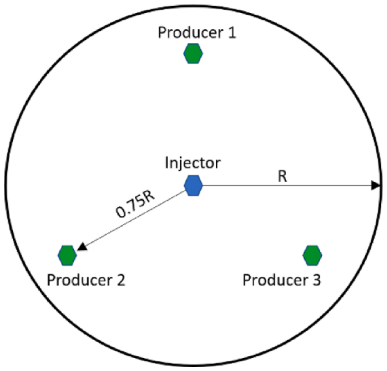

Fig. 1. Domain showing the injection and production wells; injector is located at the center and all producers are located at 0.75 R from the center where R is the radius ($R = 100$ m in this example): Example 1.

composition of the components. Additionally, this effect is reflected on the rest of the domain. To overcome these limitations, the multipoint flux approximation (MPFA) has been introduced [21–28]. Despite its advantages, MPFA involves a larger stencil leading to a denser Jacobian matrix [29] and does not necessarily produce a monotone pressure field for highly heterogeneous permeability and/or distorted cells. The mixed hybrid finite element (MFE) overcomes all of the aforementioned limitations and therefore is a natural choice for the applications presented in this paper [30–38].

The MFE is used with an implicit time scheme to solve for the pressure. The solution of the mass balance equations is based on an implicit time scheme to overcome the limitation of Courant-Friedrichs-Lewy (CFL) condition on the size of time step. The implicit solution of the transport equation in compositional two-phase flow is more complicated than single-phase flow, and immiscible two-phase flow. Different approaches have been reported in the implicit discretization of compositional two-phase flow [40–44]. The main differences in those approaches are the choice of variables and the thermodynamic constraints. Details of our implicit formulation can be found in [45,46].

CO_2 injection in subsurface formations covers a wide range of applications: CO_2 injection for enhanced oil recovery, CO_2 storage in depleted reservoirs, and CO_2 sequestration in saline aquifers. In US alone, more than 7 billion USD have been invested in CO_2 related projects [47]. When CO_2 is in contact with oil and/or water, different processes become critical in describing fluid flow. Dissolution of CO_2 both in the aqueous phase and the oil phase, and dissolution of light components of the oil phases in the CO_2-rich has phase may create density contrast that may induce different types of gravity fingering which alter fluid flow path. The authors in [48] present an experimental study to visualize the growth of fingers of CO_2 in the aqueous and oleic phases at high pressure. The model presented in [49] accounts for convective mixing of CO_2 in a single-component oil phase. Very fine grid discretization is used to observe the gravitationally induced fingers that cannot be resolved with coarse grids. In addition to gravitationally

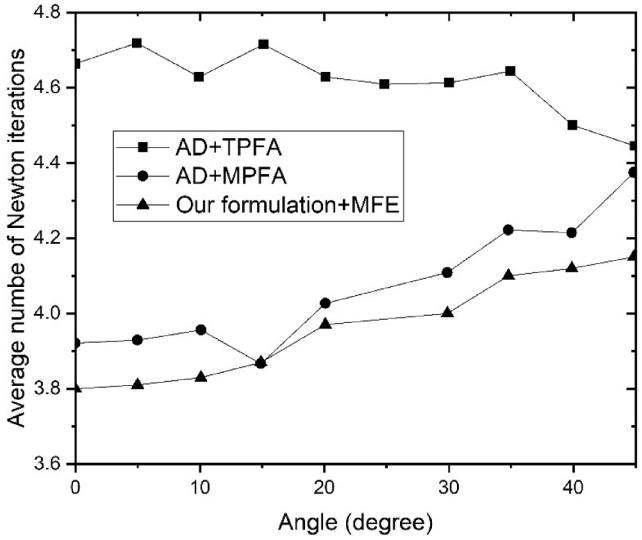

Fig. 3. Number of Newton iterations in our simulations compared to AD with TPFA and MPFA: Example 1.

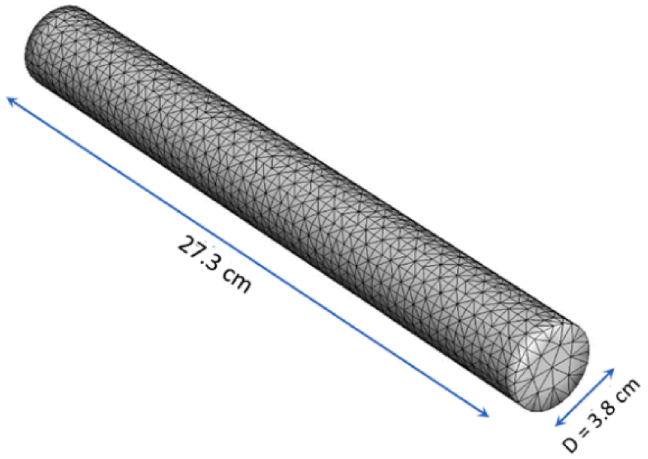

Fig. 4. Simulation domain geometry discretized with unstructured tetrahedron elements: Example 2.

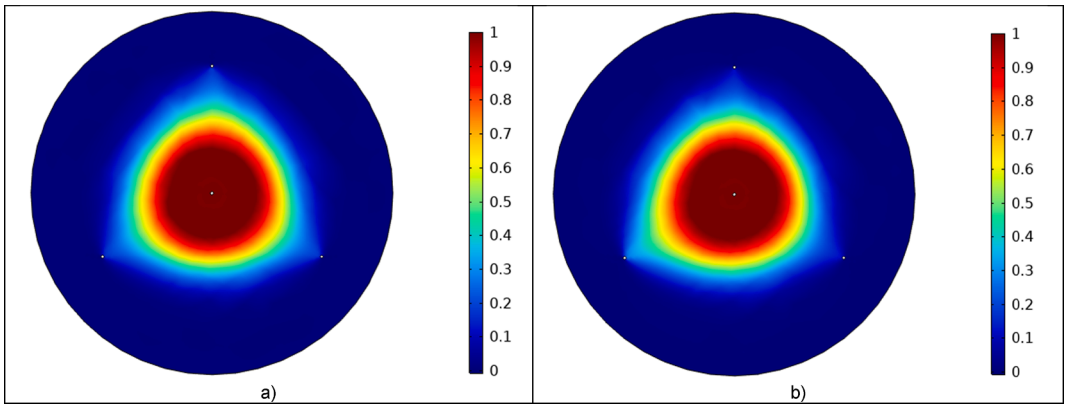

Fig. 2. CO_2 overall mole fraction with original mesh (a) and 45° perturbed mesh (b): Example 1.

Table 1
Oil composition: Example 2.

Component	Overall mole fraction
CO_2	0.0824
$N_2 + C_1$	0.5166
C_2	0.0707
C_3	0.0487
C_4-C_5	0.0414
C_6-C_9	0.0656
C_{10}-C_{14}	0.0613
C_{15}-C_{19}	0.0371
C_{20+}	0.0762

induced fingers, molecular diffusion has been shown to be an important rate-controlling mechanism in CO_2 flooding [50]. The experimental data are used to measure the diffusivity of CO_2 in hydrocarbons and water at reservoir conditions. Experimental and simulation results are presented in [51] for CO_2 injection in a chalk sample saturated with n-C_{10}. Numerical modeling of the experiment in [51] is based on the commercial simulator Eclipse 300 in 2D. The diffusion coefficients in [51] are estimated with an optimization algorithm that gives the best fit to the experimental data. In [52] laboratory, and numerical simulations are presented for CO_2 injection in a sandstone core saturated with a mixture of hexane and decane. The authors [52] use the commercial simulator CMG (Computer Modeling Group) in 2D to model the experimental data. Another study in [53] presents a numerical modeling study of gas injection followed by CO_2 injection in a chalk core based on experimental data. The core is initially saturated with synthetic oil mixture of C_1 and n-C_7. The authors [53] use two different commercial simulators, SENSOR and Eclipse 300, both applied in 2D simulations. They [53] report that both simulators give nearly the same results. In a recent work [54], experimental and numerical studies are conducted for CO_2 injection in one-meter-long tight core. Immiscible CO_2 flooding is researched in [54], and experimental results indicate that injection pressure and CO_2 diffusion are among the main parameters that affect production performance. The authors in [54] use the CMG simulator with 3D corner point grids to mimic the cylindrical shape of the core. A sensitivity analysis is conducted in relative permeability to history match the data. In [55] a lab scale simulation for CO_2 injection is studied using structured grids.

Density effects in CO_2 injection may result in frontal instabilities. In such cases, Fickian diffusion may have a drastic effect on flow path and process performance. If diffusion is neglected, early breakthrough occurs leading to low oil recovery. In addition, exchange of species by diffusion may affect phase behavior leading to higher oil recovery from swelling and/or viscosity reduction. A proper description of diffusion is critical in compositional flow. A generalized Fick's law to multicomponent mixture for instance violates molar balance in multicomponent mixture by considering a diagonal matrix of diffusion coefficients [55]. Calculation of diffusive fluxes from gradients of compositions does not describe the diffusion properly because the compositional gradients are defined within a single phase. In this work a proper description of the diffusion fluxes is presented. The adopted approach is based on the chemical potential gradients proposed. This approach does not require phase identification and diffusion fluxes could be computed across phase boundaries. In this work we introduce the idea of unstructured gridding in applications related to CO_2 injection, without adjustment and/or tuning of diffusion coefficients. We demonstrate that the physics is accurately described with the adopted diffusion model and the proper choice of grid type. The flow parameter are used without adjustment.

The rest of this paper is organized as follows. First, we provide a general description of the model and the governing equations that describe compositional two-phase flow; then three numerical examples are presented to highlight the features of our model; and finally, we end with a summary of our main conclusions.

2. Mathematical model

The mass balance of component i in compressible two-phase (gas and oil) flow of an n_c -component mixture is given by:

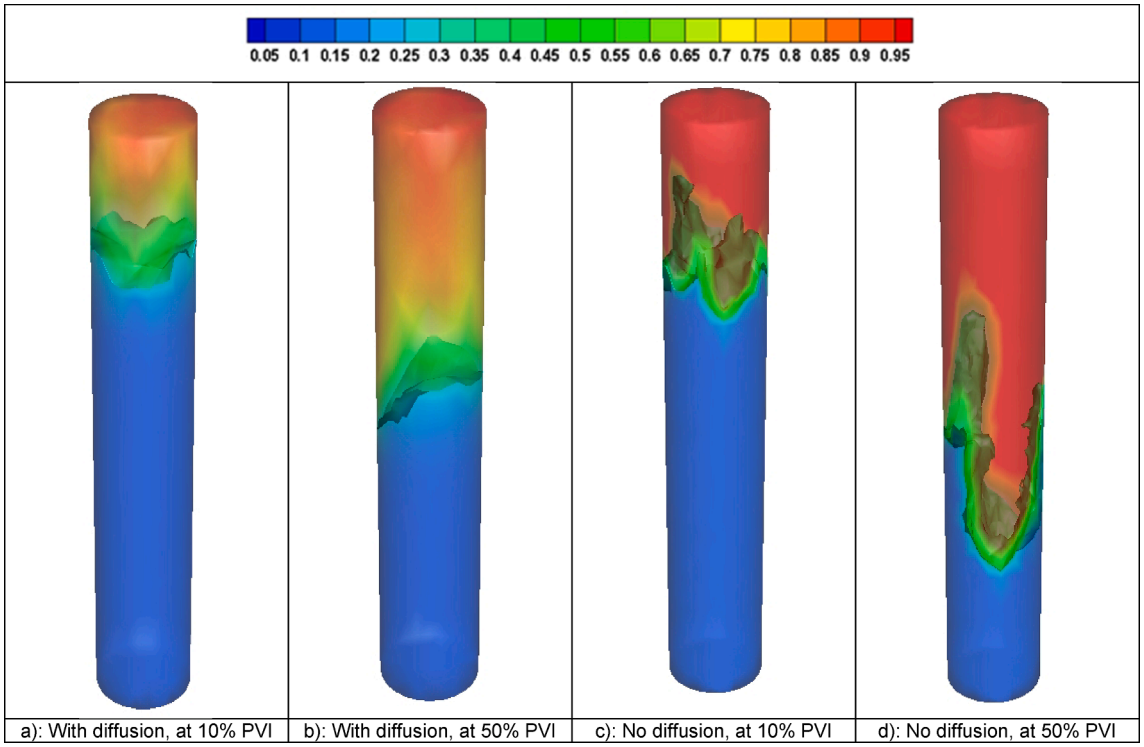

Fig. 5. CO_2 overall mole fraction at different PVI with and without Fickian diffusion: Injection from the top (11643 grids): Example 2.

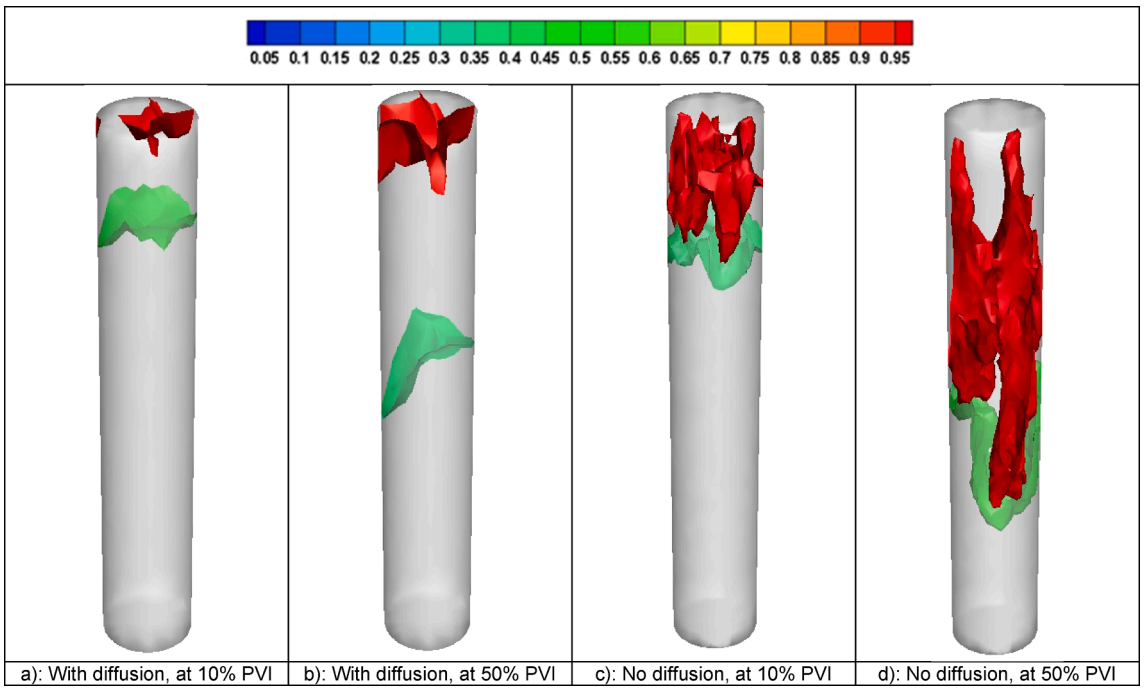

Fig. 6. Iso-surface of CO_2 overall mole fraction at different PVI with and without Fickian diffusion; injection form the top (11643 grids): Example 2.

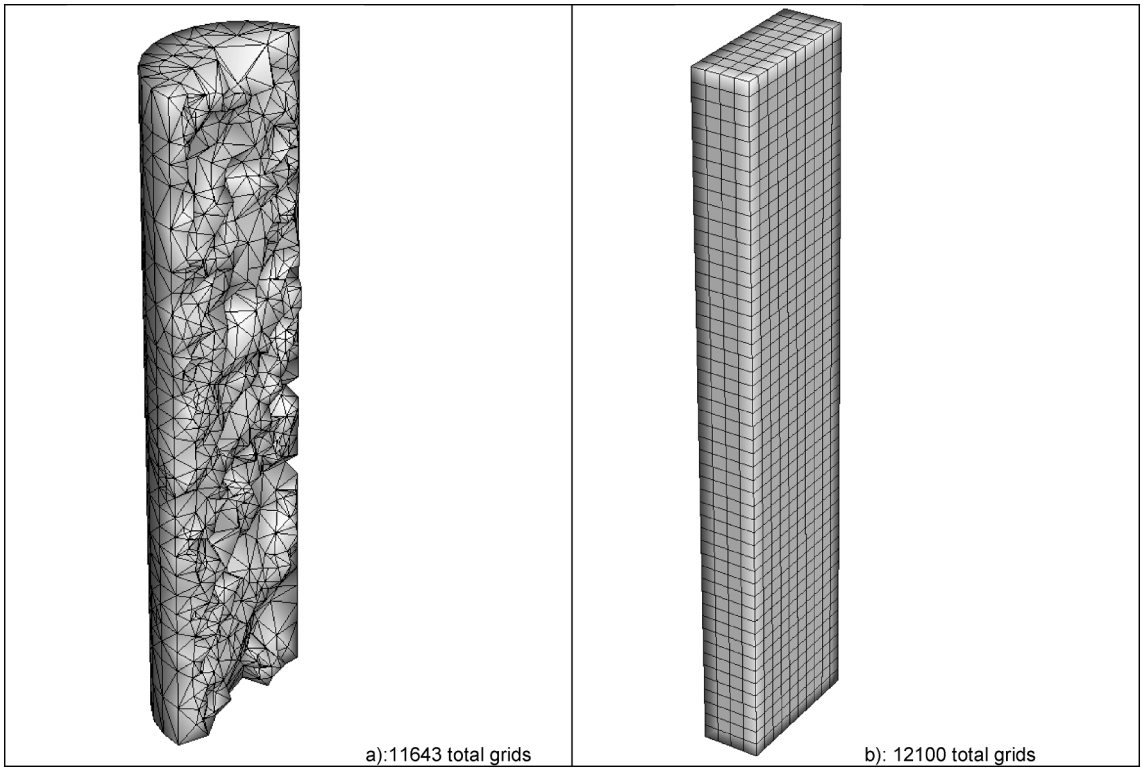

Fig. 7. Vertical cross section showing half of the domain in two different grid types, tetrahedra (a) and hexahedra (b): Example 2.

$$\phi\frac{\partial cz_i}{\partial t}+\nabla.\left(\sum_{\alpha}c_{\alpha}x_{i,\alpha}v_{\alpha}+S_{\alpha}J_{i,\alpha}\right)=F_i, i=1...n_c \text{in}\Omega\times(0,\tau) \quad (1)$$

The velocity of phase α is given by Darcy's law:

$$v_{\alpha}=-\frac{\mathbf{K}k_{r\alpha}}{\mu_{\alpha}}(\nabla p-\rho_{\alpha}g)=-\lambda_{\alpha}\mathbf{K}(\nabla p-\rho_{\alpha}g), \alpha=o,g \quad (2)$$

The pressure equation is based on the concept of total volume balance [56,57] given by:

$$\phi C_t\frac{\partial p}{\partial t}+\sum_{i=1}^{n_c}\overline{V}_i\nabla.\left(\sum_{\alpha}c_{\alpha}x_{i,\alpha}v_{\alpha}+S_{\alpha}J_{i,\alpha}\right)=\sum_{i=1}^{n_c}\overline{V}_iF_i \quad (3)$$

In the above equations, α is the phase index (gas and oil),ϕ denotes the porosity,v_{α} the velocity of phase α , c the overall molar density of the

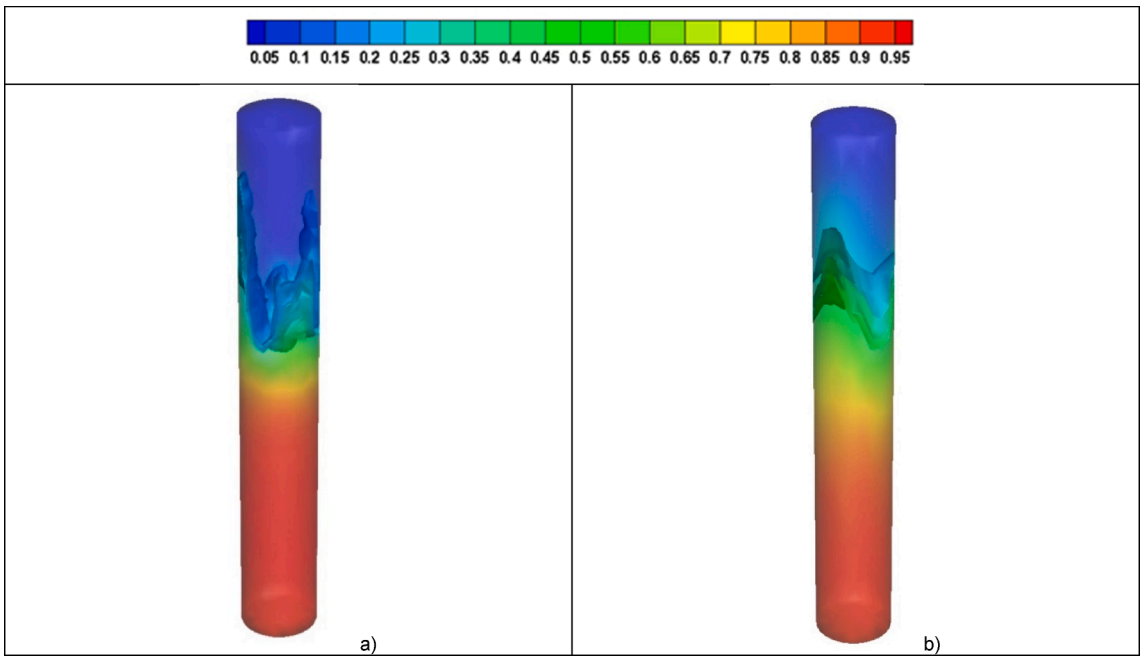

Fig. 8. CO2 overall mole fraction without diffusion (a), with diffusion (b): at 50% PV injection from the bottom (11643 grids): Example 2.

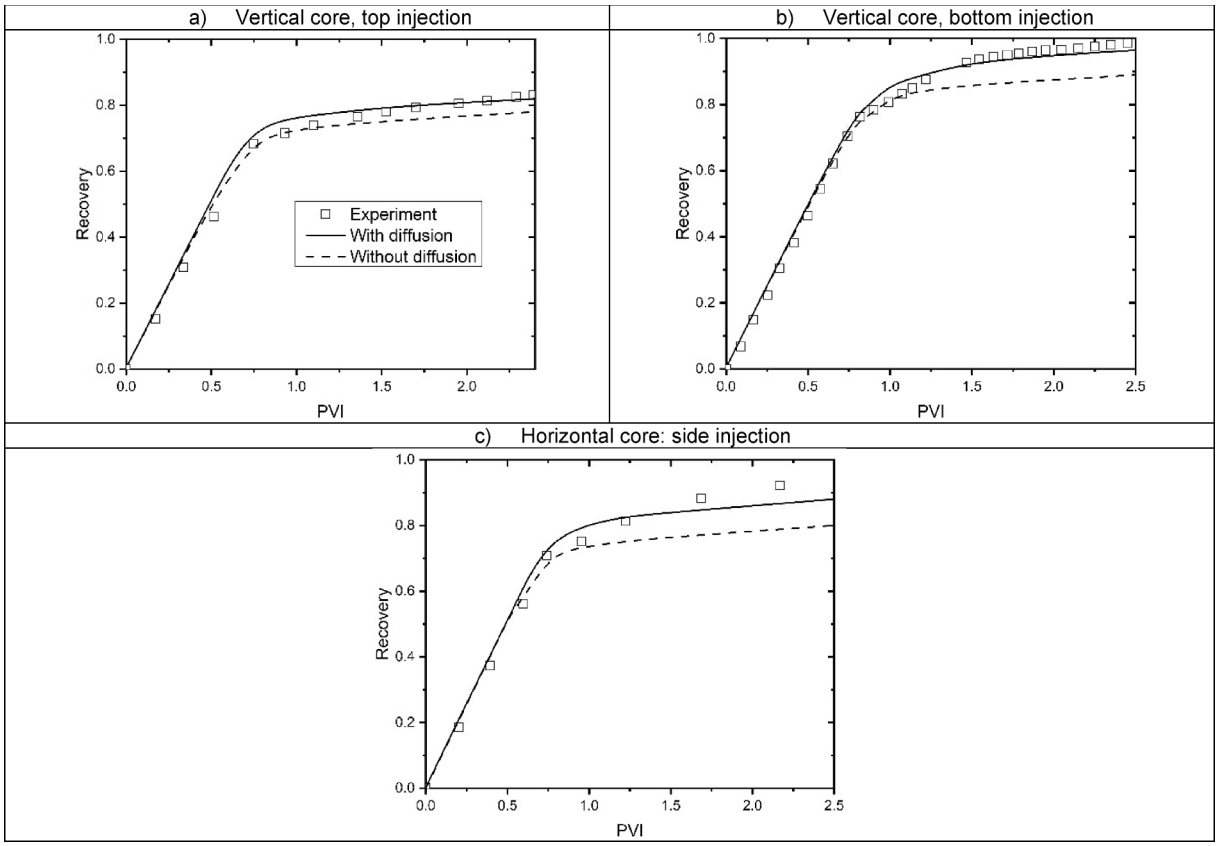

Fig. 9. Oil recovery from injection from the, top (a), bottom (b), and side (c): Example 2.

mixture, and z_i and F_i are the overall mole fraction and the sink/source term of component i in the mixture, respectively. c_α is the molar density of phase α and $x_{i,\alpha}$ is the mole fraction of component i in phase α. **K** is the absolute permeability, $k_{r\alpha}$, μ_α and ρ_α are the relative permeability, dynamic viscosity and mass density of phase α , respectively, with $\lambda_\alpha = k_{r\alpha}/\mu_\alpha$; p is the pressure and **g** is the gravitational acceleration. C_t is the total compressibility and $\overline{V}_i$ is the total partial molar volume of component i. S_α the saturation of phase α, $\boldsymbol{J}_{i,\alpha}$is the diffusive flux of component i in phase α, Ω is the computational domain andτ τ denotes the simulation time.

We calculate the variation of molar density of a component in one of

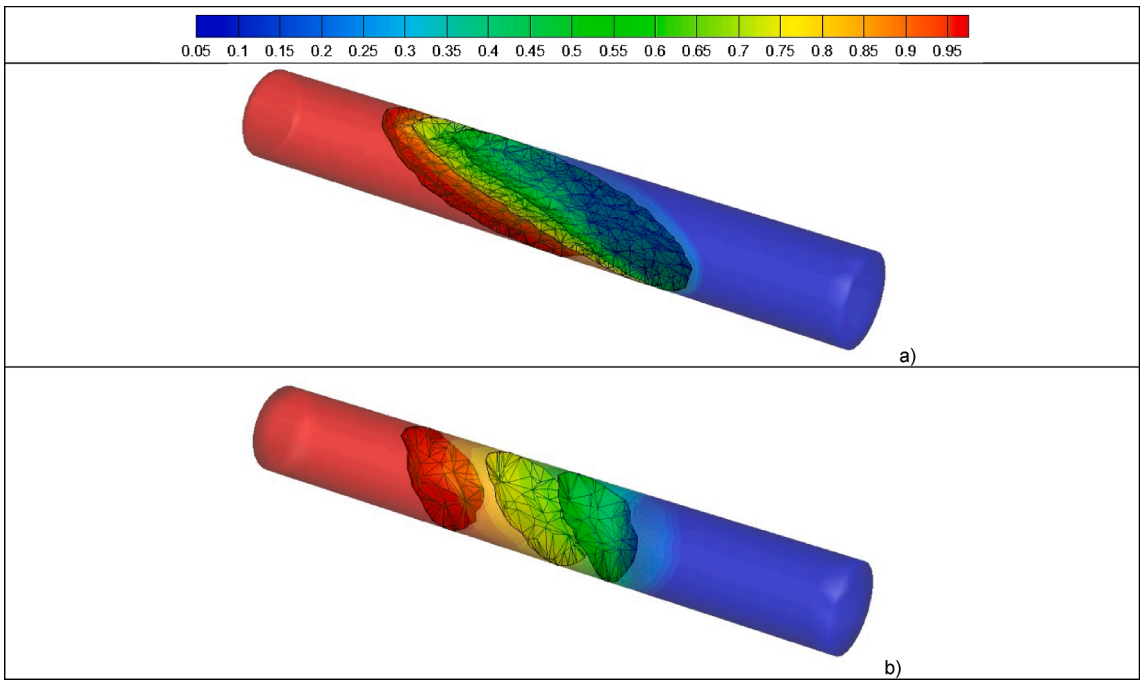

Fig. 10. CO_2 overall mole fraction without diffusion (a), with diffusion (b): at 50% PVI: Horizontal Injection (11643 grids): Example 2.

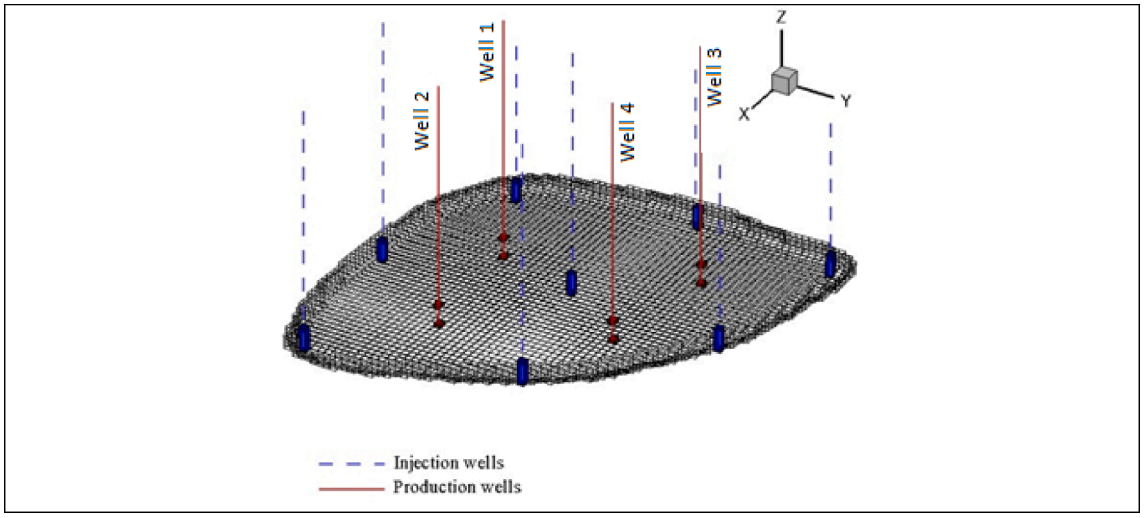

Fig. 11. The Egg domain showing locations of injection and production wells; 18,533 grids: Example 3.

the two phases with respect to the total molar density, $\partial c_{\alpha,i}/\partial c_i \partial c_{\alpha,i}/\partial c_i$ at constant volume and temperature using the equality of fugacities [58–63].

The molar Fickian diffusion flux in phase α for an n_c– component mixture is given by:

$$\boldsymbol{J}_\alpha = -\boldsymbol{D}_\alpha c_\alpha \nabla \boldsymbol{x}_\alpha \tag{4}$$

where $\boldsymbol{D}_\alpha$ is the matrix of molecular diffusion coefficients and $\boldsymbol{x}_\alpha$is the component mole fraction in phase α. The off-diagonal matrix entities in $\boldsymbol{D}_\alpha$are often set to zero, however, a realistic diffusion model should include both diagonal and off-diagonal entities [64,65]. Equation (4) cannot be used when a grid cell has only oil and the cell next to it has only gas or is in two phase state. In such conditions, we calculate the diffusive fluxes based on the chemical potential gradients as suggested in [66]. In this formulation, the driving force of the diffusion flux is the chemical potential gradient, and the diffusive flux is given as follows:

$$J_{i,\alpha} = -\frac{\phi S_\alpha c_\alpha}{RT} \sum_{j=1}^{n_c-1} x_{j,\alpha} \nabla \mu_{j,\alpha} \left(B_{i,j,\alpha}\right)^{-1} \tag{5}$$

with R the gas constant and T the temperature, $\mu_{j,\alpha}$ is the chemical potential of component j in phase α, and B is a matrix derived from the Stefan − Maxwell diffusion coefficients. The Stefan-Maxwell diffusion coefficients are calculated based on the generalized Vignes relation for infinite diluted components as follows [67]:

$$D_{i,j} = \left(D_{i,j,inf}\right)^{x_j} \left(D_{i,j,inf}\right)^{x_i} \prod_{\substack{k=1 \\ k \neq i,j}}^{n_c} \left(D_{i,k,inf} D_{j,k,inf}\right)^{x_k/2} \tag{6}$$

In the above equation $D_{i,j}$ is the Stefan-Maxwell molecular diffusion coefficient of the pair i-j and $D_{i,j,inf}$ is the molecular diffusion coefficients of component i infinitely diluted in component j. The plots in [68]

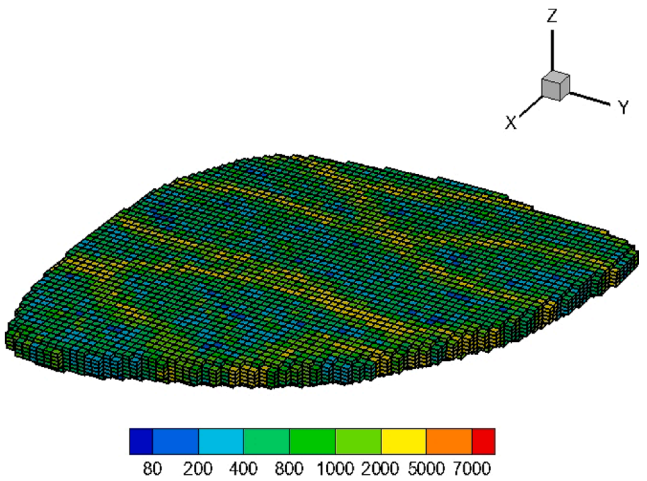

Fig. 12. K_x permeability distribution [md]: Example 3.

indicate that for a porosity higher than 20% the tortuosity is less than two; we could safely ignore the adjustment of diffusion coefficients for tortuosity in this work in relation to predictions in Example 2 to be discussed later.

The proposed formulation implies that at equilibrium condition there in no diffusion flux. This is justified by the fact that the main driving force is the chemical potential gradient. This will be demonstrated in the example presented in appendix A. Injecting a binary mixture of equilibrium gas into the same (oil) binary mixture should be unaffected by the effect of diffusion as will be shown in appendix A. Away from equilibrium, the effect of diffusion may affect flow performance.

3. Numerical discretization

We present in this section the numerical discretization scheme of the proposed model. A finite volume integration of equation (1) gives:

$$G_{K,i} = \varnothing|K|\frac{cz_{i,K}^{n+1} - cz_{i,K}^{n}}{\Delta t} + \sum_{E\in\partial K}\sum_{\alpha}(c_\alpha x_{i,\alpha}{}^{n+1} q_{\alpha,K,E} + \nabla\overline{\mu_E}) - |K|F_i = 0 \quad (7)$$

where $|K|$ is the surface area of the finite element K, $c_\alpha x_{i,\alpha}$ is the upstream value of $c_\alpha x_{i,\alpha}$, and $q_{\alpha,K,E}$ is the normal flux of phase α at the interface E of element K. The above equation is solved implicitly using the Newton-Raphson method. More details about the implicit solution of two-phase compositional flow could be found in [45]. $\nabla\overline{\mu_E}$ is the gradient of chemical potential at the interface E multiplied by $\left(B_{i,j,\alpha}\right)^{-1}\phi S_\alpha c_\alpha x_{j,\alpha}/RT\Delta x$. The phase fluxes in the equation above are evaluated with the MFE as follows:

$$q_{\alpha,K,E} = \alpha_{K,E}p_K - \sum_{E'\in\partial K}\beta_{K,E,E'}tp_{K,E'} - \gamma_{K,E} \quad (8)$$

where $\alpha_{K,E}$, $\beta_{K,E,E'}$ and $\gamma_{K,E}$ depend on the geometrical shape of the element and the mobility, see [30] for more details.

4. Numerical examples

Following we present three numerical examples to highlight the features of our algorithm. Unless mentioned otherwise, the endpoints

Table 2
Selected production wells to compare CO2 overall mole fraction: Example 3.

Well name	Coordinates triplet
Well_1	(180,124,2)
Well_2	(340,140,2)

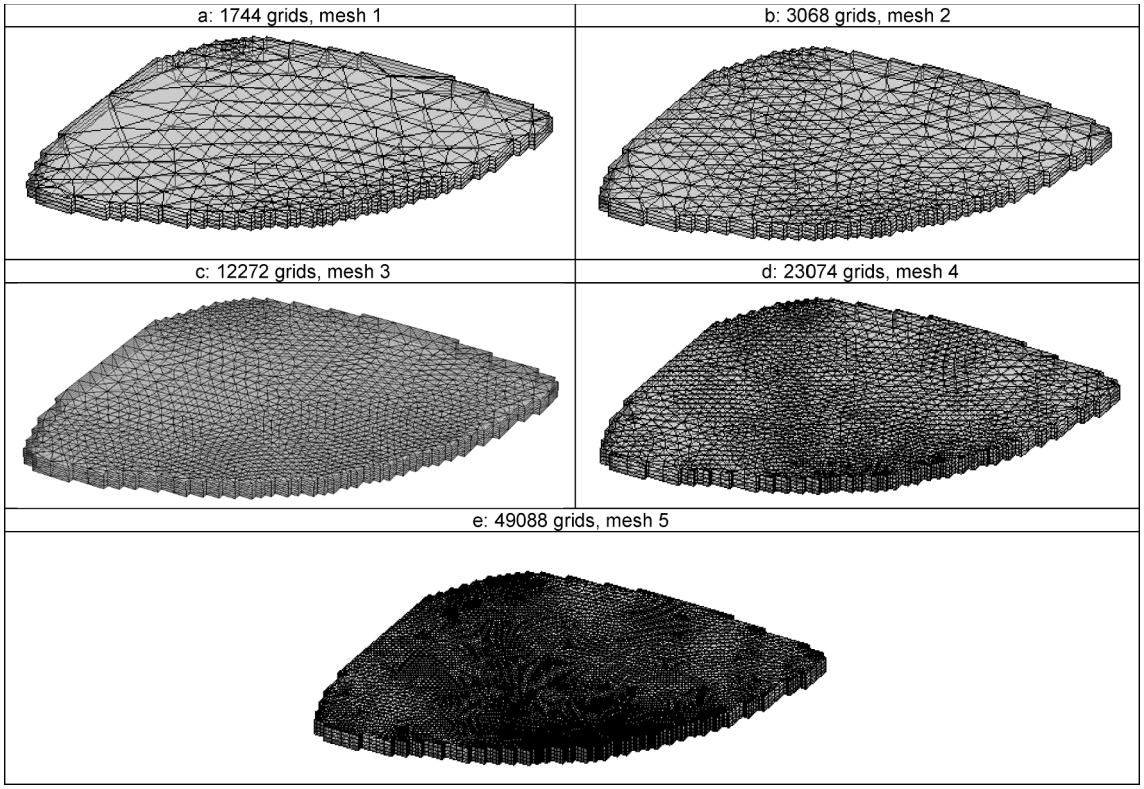

Fig. 13. Different mesh refinement with unstructured prims: Example 3.

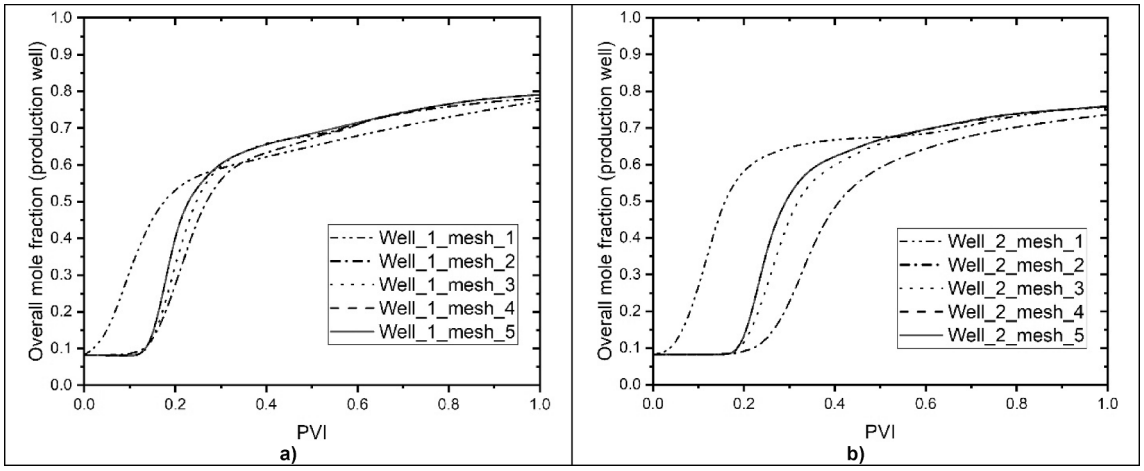

Fig. 14. Overall mole fraction of CO_2 with different mesh refinements at the producer 1 (a) and producer 2 (b): Example 3.

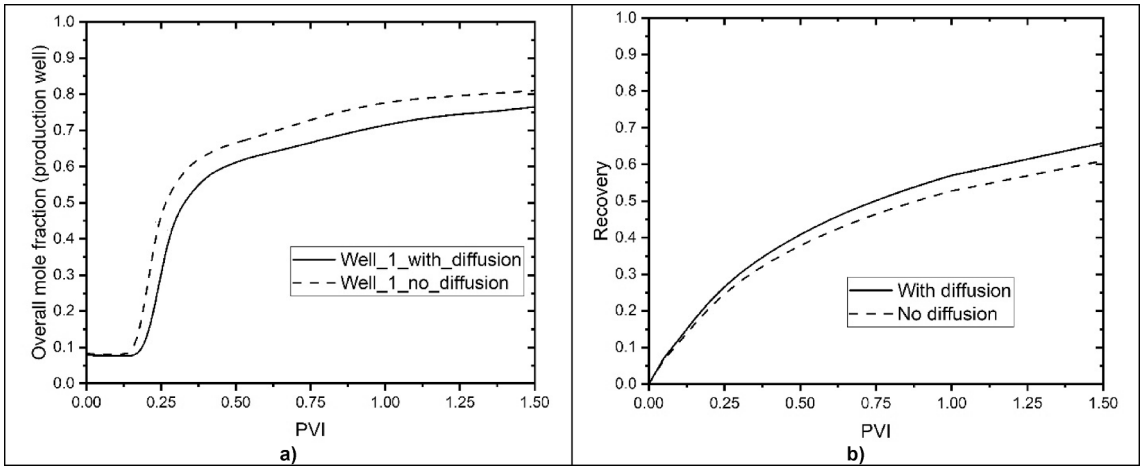

Fig. 15. Overall mole fraction of CO_2 at well_1 (a) and oil recovery (b) with and without diffusion: Example 3.

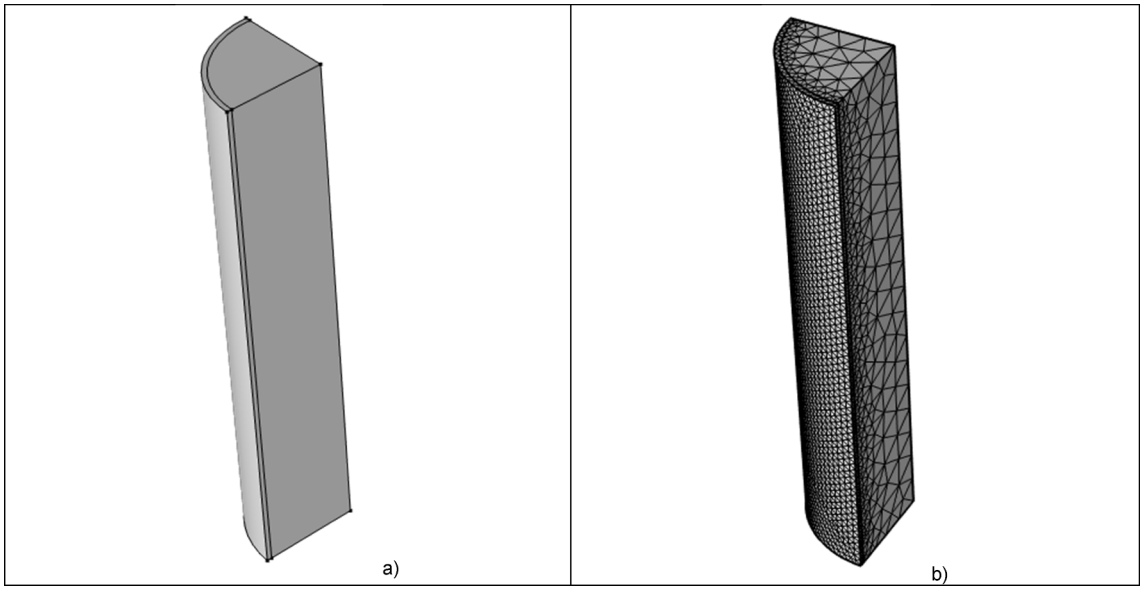

Fig. A1. Fourth of the domain (a) and the corresponding discretization mesh (b) (11431 grids).

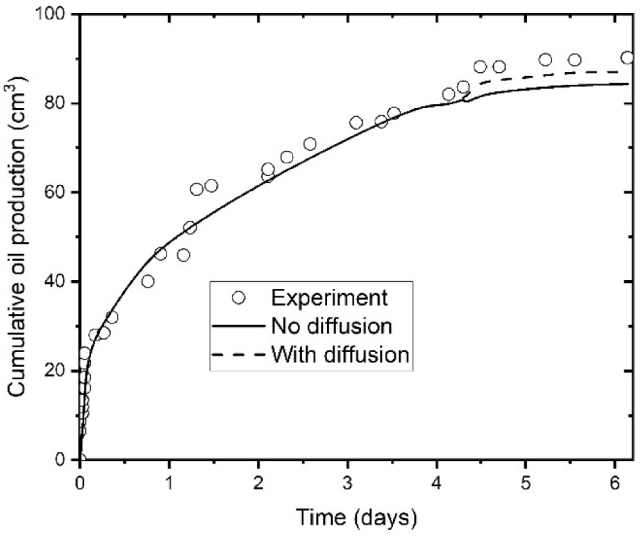

Fig. A2. Cumulative oil production with and without diffusion compared to experiment.

Table A1
Diffusion coefficient matrix in gas phase [m^2/s].

	CO_2	C_1	C_7
CO_2	2.57E-08	2.15E-10	−2.27E-12
C_1	−1.87E-08	4.22E-09	−6.33E-10
C_7	1.19E-08	1.45E-08	1.96E-08

Table A2
Diffusion coefficient matrix in oil phase [m^2/s].

	CO_2	C_1	C_7
CO_2	1.48E-08	−4.47E-11	−6.61E-12
C_1	−1.02E-08	1.99E-09	−1.25E-09
C_7	6.77E-09	9.40E-09	1.26E-08

relative permeabilities for gas and oil are 0.2 and 0.6 respectively with a power of 2 for both in all the simulations. This is justified in CO_2 injection since CO_2 alters the wettability of the rock and therefore it is assigned a lower endpoint relative permeability. Production is performed at constant pressure and injection is at constant volumetric rate in all examples. Capillary pressure is neglected in this work; this is justified by the low interfacial tension and the high solubility of CO_2 in oil. Note that the domain is assumed to be rigid; the physical properties of the domain (permeability, porosity) do not change with the variation of pressure.

4.1. Example 1: Mesh dependency

In this example we compare the effect of mesh distortion on the efficiency and accuracy of the proposed formulation. We consider CO_2 injection in a circular reservoir saturated with a mixture of 70% CO_2, 25% C_1 and 5% C_4 presented in [69]. The reservoir pressure is 125 bar and the temperature is 380 K. Injection is performed at a constant rate (100 m^3/day) at the center and production is performed at three producers equally distanced from the injector (Fig. 1). The number of Newton iterations in the implicit discretization is a measure of the efficiency of the algorithm and the proposed formulation. In [69] the automatic differentiation (AD) is used in the implicit discretization. Our implicit formulation is discussed in detail in [45]. To study the effect of gridding on the performance of the algorithm, the authors [69] consider different rotation angles of the grids towards the left producer from 0 to 45°. We consider the same study in this example and compare the number of Newton iterations obtained in our formulation using MFE discretization to AD in [69] with two discretization schemes, TPFA and MPFA. In Fig. 2 we show CO_2 overall mole fraction with the original and the 45° perturbed meshes.

In Fig. 3 we show the average number of Newton iterations in our algorithm compared to that of [69] in TPFA and MPFA. Results show the lowest number of Newton iterations are obtained in our implicit formulation using the MFE discretization compared to AD in TPFA and MPFA from [69]. Similar CO_2 profiles are obtained in the original and the perturbed mesh. The CO_2 profiles and the low number of Newton iterations demonstrate the efficiency and accuracy in addition to the low mesh dependency of the proposed algorithm.

4.2. Example 2: Fickian diffusion

We investigate the effect of Fickian diffusion and gridding in lab scale simulations in 3D. This example has been studied in 2D with structured grids [66]. In this work we use a cylindrical domain in the simulation to allow true representation of the geometry. Our simulations are based on fully unstructured 3D grids. The major motivation is that we account not only for pore volume but also cross-sectional area and randomness of diffusion. The domain/core measures 27.3 cm long with a diameter of 3.8 cm (Fig. 4). CO_2 is injected uniformly at one side at a constant rate of 1 pore volume per day (PV/D) and production is at a constant pressure of 441.3 bar at the opposite side. The temperature is held constant at 331.2 K. The permeability is 221 md and the porosity is 13%. At the given conditions, the CO_2 density is 0.92 g/cc and the oil density is 0.74 g/cc. The oil composition is given in Table 1 and details of PVT analysis of the oil are provided in [66]. The residual oil saturation is set to 10%,' when the phase behavior is strong, the residual oil saturation to CO_2 is not relevant. The density difference may create an unstable front.

We perform simulations of injection from the top and the bottom in a vertical core, and injection from the side in a horizontal core. In the simulations we investigate the effect of diffusion by considering two cases in each injection scenario, with and without Fickian diffusion. In the following we first discuss the simulation results of injection from the top.

The overall mole fraction of CO_2 in the core at different pore volume injection (PVI) is shown in Fig. 5 (with and without diffusion). The higher density of CO_2 (compared to that of the oil) makes the flow gravitationally unstable. Without Fickian diffusion, this instability creates gravitational fingers. With Fickian diffusion, the fingering becomes less severe, and the interface becomes more stable. In Fig. 6 we show two *iso*-surfaces of CO_2 overall mole fraction at different PVI with and without diffusion.

Results shown in Figs. 5 and 6 confirm that diffusion stabilizes the front which delays breakthrough, and the oil recovery performance is improved. But the fingers are not completely suppressed. Simulations in 2D geometry require significant reduction of diffusion coefficients as reported by [66]. A 3D domain, however, gives a better description of the physics. In addition, the type of grid used in 3D (unstructured tetrahedra) better describes complicated flows. In our discretization, the physics of flow is described without the need to use multipliers on the diffusion coefficients. In Fig. 7 we present a cross-section of the domain showing the grids in tetrahedra and in hexahedra meshes. The flow is dominant in the vertical direction; therefore, when hexahedron gridding is used, the horizontal interfaces of the grids are the main flow paths of the fluxes. Flux exchange between the elements is therefore dominant in the vertical adjacent elements. In this example, the same simulation is run on hexahedron grids (results not shown) and a uniform displacement is observed when Fickian diffusion is included. The unstructured tetrahedra allow for even flux distribution, leading to more accurate description of the physics compared to hexahedron grids. An excessive mesh refinement in structured mesh may describe the physics

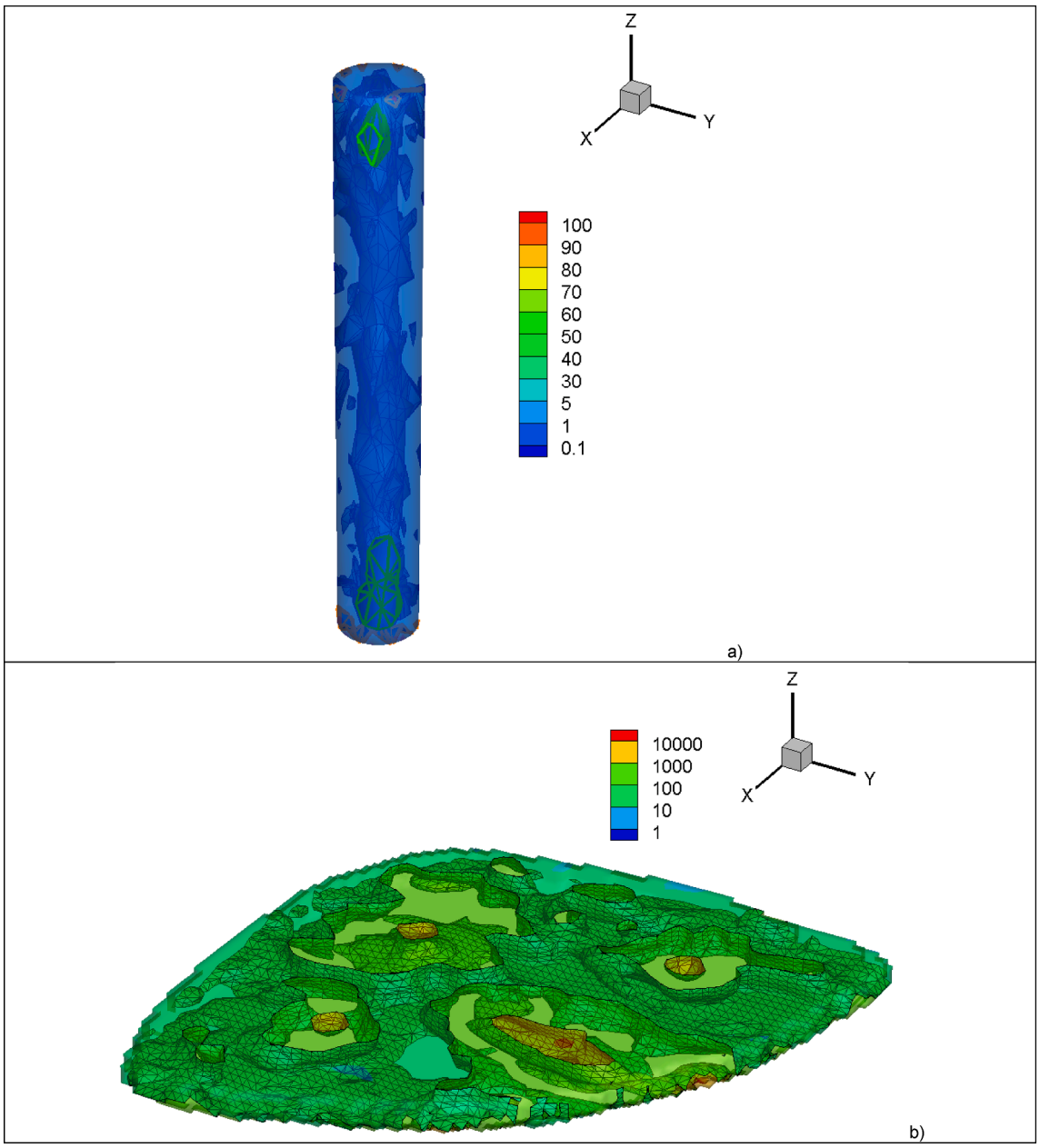

Fig. B1. Péclet number for CO_2 in example 2 (a) and example 3 (b).

accurately, however, this comes at a high computational cost. In this example, the algorithm can capture the gravitationally induced fingers with a mesh of 11,643 tetrahedron grids.

In addition to injection from the top in the vertical core we simulate injection from the bottom in the vertical core and injection form the side in the horizontal core. All other parameters are the same. Although CO_2 is heavier than the oil, when CO_2 is injected from the bottom, the evaporation of light components into the supercritical CO_2 phase leads to an unstable interface (see Fig. 8). Despite the interface instability, the recovery performance is higher in bottom injection than in top injection as shown in Fig. 9.

In horizontal injection, the density difference and low viscosity of CO_2 results in gravity segregation (see Fig. 10) and there is early breakthrough. Recovery performance in horizontal injection is higher than in top injection, and lower than the bottom injection scenario.

In order to assess the relative importance of Fickian diffusion, detailed discussion of Péclet number in compositional flow is presented in appendix B.

4.3. Example 3: Egg shape geometry

The Egg-shape permeable medium (Fig. 11) is adopted from [70]. The original domain consists of a channelized reservoir in the form of discrete permeability fields. The domain is discretized with $60 \times 60 \times 7$ structured hexahedron FE; that is a total of 25,200 elements of which 18,553 cells are active. Several publications have used the domain for different types of flow simulation [71]. The input data files of the domain are accessible to external users through Sintef repository [72]. The Egg domain contains 8 injection wells and 4 production wells. Locations of injection and production wells are shown in Fig. 11. In this example the reservoir is saturated with the 8-component oil mixture presented in Example 2 and using the same residual oil saturation. CO_2 is injected at constant rate of 5% PV/year.

The domain has a constant porosity of 20% while the permeability varies from 70 md to 7000 md. The permeability values along the x,y, and z directions are provided on Sintef website for each grid-cell in the domain. Fig. 12 shows the K_x permeability distribution.

Various authors in the literature have used the same structured hexahedron grid type [11,71,72] for the Egg shape domain. In this example the Egg domain is discretized with unstructured prisms.

We consider five different mesh refinements in Fig. 13 (between 1700 and 49,000 elements, with the latter used as a reference solution mesh; more refinement does change the results). We compare the variation of overall mole fraction of CO_2 in two production wells for all meshes. The coordinates of selected wells are given in Table 2. Results are shown in Fig. 14. In a problem with a total of 12 injection and production wells, along with the phase behavior complexity, a coarse mesh of 1700 elements gives inaccurate results (Fig. 14). A mesh refinement of 12,000 grids and above is required to produce accurate results. As shown in Fig. 14, the difference between the 12,000 grids and 23,000 grids results is small up to 0.5 PVI and becomes nearly identical above that. A relatively coarse mesh of 12,000 elements demonstrates the accuracy and efficiency of the algorithm in problems with different degrees of complexity.

To study the effect of diffusion at reservoir scale a simulation with diffusion is conducted using mesh_4. Results do not show a difference compared to the original case without diffusion. This is related to the high number of wells that makes the flow convective dominant. Despite the heterogeneity of the domain, the permeability contrast is not high enough to clearly observe the effect of Fickian diffusion. To overcome this limitation, we adjust the permeability distribution to have a lower value of 2 md, that is 35 times less than the original value. With this configuration the effect of diffusion is more pronounced. Fig. 15a shows the overall mole fraction of CO_2 at well_1 with and without diffusion. Results show how diffusion reduces the overall mole fraction of injected CO_2 at the producer which increases to oil recovery by less than 10% (Fig. 15b).

5. Concluding remarks

- We present an implicit numerical model for compositional two-phase flow in fully unstructured grids in 2D and in 3D. The algorithm provides representation of the physics of flow.
- Our algorithm shows low mesh dependency in compositional flow in CO_2 injection.
- The algorithm is demonstrated to be efficient in terms of Newton iterations in perturbed grids, partly related to our implicit formulation and partly due to the MFE discretization.
- In CO_2 injection with consideration of gravity and Fickian diffusion, use of unstructured gridding has a significant effect on accuracy of simulations. Use of Cartesian geometry and idealization might not describe the physics properly. In 3D with unstructured gridding the flow path is predicted accurately.
- In field scale, and with high permeability contrast the effect of diffusion has a positive effect on recovery and may not be ignored.

Declaration of Competing Interest

The authors declare that they have no known competing financial interests or personal relationships that could have appeared to influence the work reported in this paper.

Acknowledgement

This work was supported by the member companies of the Reservoir Engineering Research Institute (RERI) whose support is gratefully acknowledged.

Appendix A

We present numerical simulation of lab experiments from gas injection in fractured from [73]. In the experiments, a mixture of methane and n-heptane is injected. The fractured media are saturated with the same binary hydrocarbon in liquid state. The injection gas and the liquid in fractured media are in equilibrium. At the end of equilibrium gas injection after 4.2 days, CO_2 is injected for 2.2 days. In equilibrium gas injection, there should be no effect from diffusion flux despite the fact that diffusion coefficients are not zero. In CO_2 injection, we should expect diffusion effect on recovery. However, because of closeness to the critical point the effect may not be pronounced as established from theory [74]. The IFT value of the binary is 0.15 mN/m, for the ternary mixture the IFT is even lower at 0.08 mN/m. These are calculated based on parachors and verified with the measured data in [73]. The IFT values are at the pressure and temperature conditions of the experiments.

The domain consists of a chalk core of 19.6 cm length and 3.8 cm diameter. The core permeability is 5 md and has a porosity of 44%. The fracture surrounds the core. Details of the creation of this fracture are given in [73]. Fig. A1 shows the domain and the discretization mesh of one fourth of the simulation domain. We use the same relative permeabilities as those described in the main text.

Fig. A2 presents the oil recovery from our simulations with and without diffusion. In the period of equilibrium gas injection there is no contribution from diffusion as expected. In CO_2 injection diffusion may contribute to recovery, however the effect may not be pronounced close to the critical point. In Tables A1 and A2 we list the full diffusion coefficient matrix in both oil and gas phases.

Reference [53] presents the simulation of the data from [73]. Unlike our simulations in which there is no adjustment of data, the authors adjust the injection rate of hydrocarbon injection; they reduce the injection rate from 0.1 cm^3/min to 0.0386 cm^3/min for 0.068 days. In the CO_2 injection, the rate is increased from 0.1 cm^3/min to 0.364 cm^3/min for 0.3 days and then reduced to 0.07 cm^3/min. Our simulation results are in agreement with the data. The measured recovery from CO_2 injection is somewhat higher than our predictions. We believe the measured data show the true trend. In our work we neglect capillary pressure. There is a small reduction in capillary pressure from CO_2 injection because of the reduction in interfacial tension. The reduction in capillary pressure may result in increase in recovery. When diffusion coefficients are small, the effect of diffusion becomes less significant, but cannot be neglected as opposed to what is reported in the literature.

Appendix B

In high permeability rocks the advection process usually dominates over the diffusion [75]. In such cases the Fickian diffusion may be neglected in in the simulations. In other applications, the diffusion effect might not be negligible. The dimensionless Péclet number provides a measuring tool to assess the relative importance of the molecular diffusion. Péclet number in 1D single-phase flow is given as follows:

$$P_e = \frac{vL}{D} \tag{7}$$

where v is the velocity, L is the characteristic length and D is the diffusion coefficient. In 3D there is no well-established approximation of the above

equation for multiphase multicomponent compositional flow. In this work we present a modified approach for Péclet number for CO_2 in 3D for compositional two-phase flow as follows:

$$P_{ei} = max\left[abs\left(\left(\frac{v_{x\alpha}L_x}{D_{i\alpha}}, \frac{v_{y\alpha}L_y}{D_{i\alpha}}, \frac{v_{z\alpha}L_z}{D_{i\alpha}}\right)\right)\right] | \alpha = o, g; i = 1..n_c$$

In the above equation Péclet number is computed for each component i in phase α from the maximum velocity component along the three axes x, y and z.

In Fig. B1 we show Péclet number for CO_2 in Example 2 (injection from the top) and Example 3. Results show that in most of the domain in Example 2 the Péclet number for CO_2 is less than one. In contrast, for Example 3 Péclet number is higher than one and reaches a maximum of more than 10,000 in some parts of the domain. This is because of high flowrate and the effect of multiple injection and production wells on the convective flow.

References

[1] Jackson M, Percival J, Mostaghimi P, Tollit B, Pavlidis D, Pain C, Blunt M. Reservoir modeling for flow simulation by use of surfaces, adaptive unstructured meshes, and an overlapping-control-volume finite-element method. Society of Petroleum Engineers; 2015, doi.10.2118/163633-PA.

[2] Mlacnik M, Durlofsky LJ, Heinemann ZE. Sequentially adapted flow-based PEBI grids for reservoir simulation. Society of Petroleum Engineers; 2006, doi:10.2118/90009-PA.

[3] Wu X-H, Parashkevov R. Effect of grid deviation on flow solutions. Society of Petroleum Engineers; 2009, doi:10.2118/92868-PA.

[4] Mifflin RT, Watts JW, Weiser A. A fully coupled, fully implicit reservoir simulator for thermal and other complex reservoir processes. In: Paper SPE 21252 presented at the SOE symposium on reservoir simulation; 1991, Anaheim, California. doi: 10.2118/21252-MS.

[5] Watts JW, Shaw JS. A new method for solving the implicit reservoir simulation matrix equation. In: Paper SPE 93068 presented at the SPE reservoir simulation symposium; 2005, The Woodlands, Texas. doi: 10.2118/93068-MS.

[6] Naccache PF. A fully implicit thermal reservoir simulator. In: Paper SPE 37985 presented at the SPE reservoir simulation symposium, Dallas; 1997. doi:10.2118/37985-MS.

[7] Beckner BL, Usadi AK, Ray MB, Diyankov OV. Next generation reservoir simulation using russian linear solvers. In: Paper SPE 103578 presented at the SPE Russian Oil and gas technical conference and exhibition, Moscow; 2006, doi:10.2118/103578-MS.

[8] Usadi A, Mishev I, Shaw J, Wiegand K. Parallelization on unstructured grids. In: Paper SPE 106063 presented at the SPE reservoir simulation symposium, Houston; 2007, doi: 10.2118/106063-MS.

[9] Karypis G, Kumar V. METIS 4.0. Unstructured graph partitioning and sparse matrix ordering system. Technical report. Minneapolis, Minnesota: University of Minnesota; 1998.

[10] Liu K, Subramanian G, Dratler DI, Lebel J-P, Yerian JA. A general unstructured-grid, equation-of-state-based, fully implicit thermal simulator for complex reservoir processes. Society of Petroleum Engineers; 2009, doi:10.2118/106073-PA.

[11] Moortgat Joachim, Firoozabadi Abbas. Mixed-hybrid and vertex-discontinuous-Galerkin finite element modeling of multiphase compositional flow on 3D unstructured grids. J Comput Phys 2016;315:476–500.

[12] Vestergaard H, Olsen H, Sikandar AS, Abdulla IA, Noman R. The Application of Unstructured-Gridding Techniques for Full-Field Simulation of a Giant Carbonate Reservoir Developed with Long Horizontal Wells. Society of Petroleum Engineers; 2008, doi:10.2118/120887-PA.

[13] Nacul EC. Use of domain decomposition and local grid refinement in reservoir simulation. PhD dissertation, Department of Petroleum Engineering; 1991, Stanford University, Stanford, California.

[14] Evazi M, Mahani H. Unstructured-coarse-grid generation using background-grid approach. Society of Petroleum Engineers; 2010, doi:10.2118/120170-PA.

[15] Kocberber S. An automatic unstructured grid generation system for geologically complex reservoirs. Society of Petroleum Engineers; 1995, doi:10.2118/28245-PA.

[16] Salinas P, Pavlidis D, Xie Z, Osman H, Pain CC, Jackson MD. A discontinuous control volume finite element method for multi-phase flow in heterogeneous porous media. J Comput Phys 2018;352:602–14.

[17] Verma SK, Aziz K. A control volume scheme for flexible grids in reservoir simulation. In: Paper SPE 37999 presented at the SPE reservoir simulation symposium, Dallas; 1997, doi: 10.2118/37999-MS.

[18] Mallison B, Sword C, Viard T, Milliken W, Cheng A. Unstructured cut-cell grids for modeling complex reservoirs. Society of Petroleum Engineers; 2014, doi:10.2118/163642-PA.

[19] Edwards Michael G, Zheng Hongwen. Quasi-positive families of continuous Darcy-flux finite volume schemes on structured and unstructured grids. J Comput Appl Math 2010;234(7):2152–61.

[20] Kozdon J, Mallison B, Gerritsen M, Chen W. Multidimensional upwinding for multiphase transport in porous media, SPE J 2011;16:263–72. SPE Reservoir Simulation Symposium, The Woodlands, TX,.

[21] Huggenberger P, Zidane A, Zechner E, Gechter D. The role of tectonic structures and density-driven groundwater flow for salt karst formation. Eng Geol Soc Territory 2015;5:609–12.

[22] Fernandes Bruno Ramon Batista, Marcondes Francisco, Sepehrnoori Kamy. Investigation of several interpolation functions for unstructured meshes in conjunction with compositional reservoir simulation. Numer Heat Tr 2013;64(12):974–93.

[23] Nordbotten JM, Aavatsmark I, Eigestad GT. Monotonicity of control volume methods. Numer Math 2007;106(2):255–88.

[24] Younes Anis, Fahs Marwan, Belfort Benjamin. Monotonicity of the cell-centred triangular MPFA method for saturated and unsaturated flow in heterogeneous porous media. J Hydro 2013;504:132–41.

[25] Younes Anis, Fahs Marwan, Zidane Ali, Huggenberger Peter, Zechner Eric. A new benchmark with high accurate solution for hot–cold fluids mixing. Heat Mass Transf 2015;51(9):1321–36.

[26] Aavatsmark I, Eigestad GT, Heimsund BO, Mallison BT, Nordbotten JM, Qian E. A new finite-volume approach to efficient discretization on challenging grids. SPE J 2010;15:658–69.

[27] Matringe SF, Juanes R, Tchelepi HA. A new mixed finite element and its related finite volume discretization on general hexahedral grids. Mech Sol Struct Fluids 2009;12:77–87.

[28] Salama A, Sun S, El Amin MF. A multipoint flux approximation of the steady-state heat conduction equation in anisotropic media. J Heat Transfer 2013;135(4):041302.

[29] Hassanpour RM, Manchuk JG, Leuangthong O, Deutsch CV. Calculation of permeability tensors for unstructured gridblocks. Society of Petroleum Engineers; 2010, doi:10.2118/141305-PA.

[30] Mosé R, Siegel P, Ackerer P, Chavent G. Application of the mixed hybrid finite element approximation in a ground water flow model: luxury or necessity? Water Resour Res 1994;30(11):3001–12.

[31] Ackerer Philippe, Younes Anis. Efficient approximations for the simulation of density driven flow in porous media. Adv Water Resour 2008;31(1):15–27.

[32] Younes A, Konz M, Fahs M, Zidane A, Huggenberger P. Modelling variable density flow problems in heterogeneous porous media using the method of lines and advanced spatial discretization methods. Math Comput Simul 2011;81(10):2346–55.

[33] Younes A, Markadi A, Zidane A, Shao Q, Bouhala L. A combination of Crouzeix-Raviart, Discontinuous Galerkin and MPFA methods for buoyancy-driven flows. Int J Numer Meth Heat Fluid Flow 2014;24(3):735–59.

[34] Zidane Ali, Younes Anis, Huggenberger Peter, Zechner Eric. The Henry semi-analytical solution for saltwater intrusion with reduced dispersion. Water Resour Res 2012;48(6). https://doi.org/10.1029/2011WR011157.

[35] Zidane Ali, Zechner Eric, Huggenberger Peter, Younes Anis. On the effects of subsurface parameters on evaporite dissolution (Switzerland). J Contam Hydrol 2014;160:42–52.

[36] Zidane A, Zechner E, Huggenberger P, Younes A. Simulation of rock salt dissolution and its impact on land subsidence. Hydrol Earth Syst Sci 2014;18(6):2177–89.

[37] Zidane Ali, Firoozabadi Abbas. An efficient numerical model for multicomponent compressible flow in fractured porous media. Adv Water Resour 2014;74:127–47.

[38] Fahs Marwan, Koohbor Behshad, Belfort Benjamin, Ataie-Ashtiani Behzad, Simmons Craig, Younes Anis, et al. A generalized semi-analytical solution for the dispersive henry problem: effect of stratification and anisotropy on seawater intrusion. Water 2018;10(2):230. https://doi.org/10.3390/w10020230.

[39] Si H. TetGen. A quality tetrahedral mesh generator and a 3D Delaunay Triangulator, http://wias-berlin.de/software/tetgen/ (2011).

[40] Fussell LT, Fussell DD. An iterative technique for compositional reservoir models. Society of Petroleum Engineers; 1979, doi:10.2118/6891-PA.

[41] Coats KH. An equation of state compositional model. J Pet Tech 1980;20(5):363–76. SPE-8284-PA. doi: 10.2118/8284-PA.

[42] Chien MCH, Lee ST, Chen WH. A new fully implicit compositional simulator. Society of Petroleum Engineers 1985. https://doi.org/10.2118/13385-MS.

[43] Naimi-Tajdar R, Han C, Sepehrnoori K, Arbogast TJ, Miller MA. A fully implicit, compositional, parallel simulator for IOR processes in fractured reservoirs. SPE; 2007. doi:10.2118/100079-PA.

[44] Voskov DV, Tchelepi HA, Younis R. General nonlinear solution strategies for multiphase multicomponent EoS based simulation. SPE; 2009, doi:10.2118/118996-MS.

[45] Zidane Ali, Firoozabadi Abbas. An implicit numerical model for multicomponent compressible two-phase flow in porous media. Adv Water Resour 2015;85:64–78.

[46] Zidane A, Firoozabadi A. Fracture-cross-flow equilibrium in compositional two-phase reservoir simulation. Society of Petroleum Engineers; 2017, doi:10.2118/184402-PA, 950-970.

[47] Hadlow RE. Update of industry experience with CO2 injection. In: Paper presented at the SPE Annual Technical Conference and Exhibition (1992), Washington, D.C.; October 1992. doi: https://doi.org/10.2118/24928-MS.

[48] Khosrokhavar R, Elsinga G, Farajzadeh R, Bruining H. Visualization and investigation of natural convection flow of CO2 in aqueous and oleic systems. J Petrol 2014. doi.org/10.1016/j.petrol.2014.07.016.
[49] Both J, Gasda S, Aavatsmark I, Kaufmann R. Gravity-driven convective mixing of CO2 in oil. In: The third sustainable earth sciences conference and exhibition 2015: 1–5, doi.org/10.3997/2214-4609.201414266.
[50] Grogan AT, Pinczewski VW, Ruskauff Gregory J, Orr FM. Diffusion of CO2 at reservoir conditions: models and measurements. SPE Res Eng 1988;93–102. doi.org/10.2118/14897-PA.
[51] Ghasemi M, Astutik W, Alavian SA, Whitson CH, Sigalas L, Olsen D, Suicmez VS. Laboratory tests and modeling of carbon dioxide injection in chalk with fracture/matrix–transport mechanisms. SPE Res Eval Eng 2018;21:122–36. doi: https://doi.org/10.2118/180102-PA.
[52] Kamali F, Hussain F, Cinar Y. A laboratory and numerical-simulation study of co-optimizing CO2 storage and CO2 enhanced oil recovery. SPE J 2015;20:1227–37. doi: https://doi.org/10.2118/171520-PA.
[53] Alavian SA, Whitson CH. Numerical modeling CO2 injection in a fractured chalk experiment. J Petrol Sci Eng 2011;77(2):172–82.
[54] Zhou Xiang, Yuan Qingwang, Zhang Yizhong, Wang Hanyi, Zeng Fanhua, Zhang Liehui. Performance evaluation of CO2 flooding process in tight oil reservoir via experimental and numerical simulation studies. Fuel 2019;236:730–46.
[55] Moortgat JB, Firoozabadi A. Fickian diffusion in discrete-fractured media from chemical potential gradients and comparison to experiment. Energy Fuels 2013;27:5793−805, dx.doi.org/10.1021/ef401141q.
[56] Acs G, Doleschall S, Farkas E. General purpose compositional model. SPE J 1985;25(4):543–53.
[57] Watts JW. A compositional formulation of the pressure and saturation equations. SPE Res Eng 1986;1(3):243–52; Trans., AIME, 281.SPE-12244-PA. doi: 10.2118/12244-PA.
[58] Zidane A, Firoozabadi A. Reservoir simulation of fractured media in compressible single-phase multicomponent in 2D, 2.5 D and 3D unstructured gridding. Adv Water Resour 2018;121:68–96. https://doi.org/10.1016/j.advwatres.2018.08.005.
[59] Zidane A, Firoozabadi A. Efficient simulation of two-phase compositional flow in fractured reservoirs using 3D unstructured gridding in complex geometries. Society of Petroleum Engineers; 2018b, doi:10.2118/191405-MS.
[60] Zidane A, Firoozabadi A. Reservoir simulation of planar and non-planar fractures in compositional two-phase flow. Society of Petroleum Engineers 2018. https://doi.org/10.2118/193117-MS.
[61] Zidane A, Firoozabadi A. Fracture cross-flow equilibrium in simulation of three-phase compositional flows. Society of Petroleum Engineers 2019. https://doi.org/10.2118/195890-MS.
[62] Zidane A, Firoozabadi A. Two-phase compositional flow simulation in complex fractured media by 3D unstructured gridding with horizontal and deviated wells. Society of Petroleum Engineers; 2019b, doi:10.2118/191405-PA.
[63] Zidane Ali, Firoozabadi Abbas. Higher-order simulation of two-phase compositional flow in 3D with non-planar fractures. J Comput Phys 2020;402:108896. https://doi.org/10.1016/j.jcp.2019.108896.
[64] Ghorayeb Kassem, Firoozabadi Abbas. Molecular, pressure, and thermal diffusion in nonideal multicomponent mixtures. AIChE J 2000;46(5):883–91. https://doi.org/10.1002/(ISSN)1547-590510.1002/aic.v46:510.1002/aic.690460503.
[65] Hoteit H, Firoozabadi A. Numerical modeling of diffusion in fractured media for gas injection and recycling schemes. SPE J 2009;14(2):323–37. SPE-103292-PA. https://doi.org/10.2118/103292-PA.
[66] Moortgat JB, Firoozabadi A, Li Z, Espósito RO. CO2 injection in vertical and horizontal cores: measurements and numerical simulation. Society of Petroleum Engineers; 2013b, doi:10.2118/135563-PA.
[67] Leahy-Dios Alana, Firoozabadi Abbas. Unified model for nonideal multicomponent molecular diffusion coefficients. AIChE J 2007;53(11):2932–9.
[68] Lala Amir MS. A novel model for reservoir rock tortuosity estimation. J Petrol Sci Eng 2020;192:107321. https://doi.org/10.1016/j.petrol.2020.107321.
[69] Zhou Y, Tchelepi HA, Mallison BT. Automatic differentiation framework for compositional simulation on unstructured grids with multi-point discretization schemes. Society of Petroleum Engineers 2011. https://doi.org/10.2118/141592-MS.
[70] Zandvliet MJ, Bosgra OH, Van den Hof PMJ, Jansen JD, Kraaijevanger. JFBM: Bang-bang control and singular arcs in reservoir flooding. J Petrol Sci Eng 2007;58:186–200. https://doi.org/10.1016/j. petrol.2006.12.008.
[71] Van Essen, G, Zandvliet M, Van den Hof P, Bosgra O, Jansen J-D. Robust waterflooding optimization of multiple geological scenarios. Society of Petroleum Engineers; 2009, doi:10.2118/102913-PA.
[72] Jansen JD, Fonseca RM, Kahrobaei S, Siraj MM, Van Essen GM, Van den Hof PMJ. Geosci Data J 2014;1:192–5. https://doi.org/10.1002/gdj3.21.
[73] Karimaie H. Aspects of water and gas injection in fractured reservoir. PhD Dissertation, NTNU, Trondheim, Norway; 2007.
[74] Firoozabadi A. Thermodynamics and applications of hydrocarbons energy production. McGraw-Hill 2015. Professional.
[75] Tian Y, Zhang C, Lei Z, Yin X, Kazemi H, Wu Y-S. An improved multicomponent diffusion model for compositional simulation of fractured unconventional reservoirs. Society of Petroleum Engineers 2021;1–26, SPE-204010-PA.